Measuring Focal Length Variations of VGOS Telescopes Using Unmanned Aerial Systems

Measuring Focal Length Variations of VGOS Telescopes Using Unmanned Aerial Systems

M. Lösler, C. Eschelbach, R. Haas, A. Greiwe

Abstract VLBI radio telescopes are large technical facilities whose structures are affected by several deformation patterns. In particular, temperature- and gravity-dependent deformations bias the estimated global telescope position and, therefore, if uncorrected, deteriorate the geodetic results that can be derived from the geodetic VLBI analysis. The rigidity of a telescope structure under varying acting forces is restricted by its structural properties. Large conventional radio telescopes are more affected by deformation effects than the new compact-designed VGOS antennas. The design document for the next generation VLBI system (today called VGOS) states <300 µm as requirement for the path length stability. A traceable metrological system that can be used to check this stability level must be at least three times better than the requirements. Close range photogrammetric methods fulfil these accuracy requirements but usually need a crane during the survey of a telescope. To avoid the latter, an unmanned aerial system was used for the first time to evaluate the possible deformation of the main reflector surface of the north-eastern of the Onsala twin telescopes (ONSA13NE). The focal length of the ring-focus paraboloid was derived in several elevation angles to study the gravitational deformation effects on the main reflector of this VGOS antenna.

Keywords VGOS · Ring-focus paraboloid · Antenna deformation · Focal length · Unmanned aircraft system

Michael Lösler · Cornelia Eschelbach
Frankfurt University of Applied Sciences, Laboratory for Industrial Metrology, Nibelungenplatz 1, DE-60318 Frankfurt am Main, Germany

Rüdiger Haas
Chalmers University of Technology, Onsala Space Observatory, SE-439 92 Onsala, Sweden

Ansgar Greiwe
University of Applied Sciences Bochum, Lennershofstraße 140, DE-44801 Bochum, Germany

(Correspondence: michael.loesler@fb1.fra-uas.de)

1 Introduction

The backbone of the next generation geodetic VLBI system will be formed by a new designed type of radio telescopes. These new radio telescopes, often refereed to as VGOS[1] radio telescopes, are of a more compact design and are able to move faster than conventional radio telescopes. One of the most important advantages of the compact design is the stability of the telescope structure against acting forces. However, radio telescopes are large technical facilities and the rigidity is restricted by structural properties. Known deformation patterns of conventional radio telescopes like thermal expansions (e.g. Haas et al., 1999), seasonal variations (e.g. Mähler et al., 2018) or gravitational sags (e.g. Bergstrand et al., 2018) can be fully transferred to the VGOS generation of radio telescopes, but have partly smaller amplitudes. Moreover, most of the VGOS radio telescopes make use of an improved main reflector design, i.e., the ring-focus paraboloid. Hence, measurement methods and mathematical models, which were suitable for conventional radio telescope, are not necessarily applicable for VGOS.

Thermal and seasonal variations of VGOS antennas have been investigated and modeled (e.g. Lösler et al., 2013; Mähler et al., 2018). However, gravitational de-

[1] VLBI Global Observing System

formations of the main reflector are not studied in detail so far. In this investigation, the focal length variations of ONSA13NE, the north-eastern of the Onsala twin telescopes, is derived to analyse the deformation behavior of a VGOS antenna. Moreover, an unmanned aerial system (UAS) is used to observe the main reflector in several elevation angles, for the first time.

2 UAS-based observation strategy

Close range photogrammetry has a long history in radio telescope surveying, dating back to the early 1960s (e.g. Findlay, 1964). Usually, photogrammetric methods are used to adjust the panels of the main reflector (e.g. Süß et al., 2012). On the one hand, advantages are the achievable uncertainties of $\ll 100\,\mu m$ for discrete signaled markers and no heavy equipment has to be mounted onto the telescope which may cause further deformations. On the other hand, a large crane is needed to retrieve a block configuration with suitable camera positions in several elevation angles of the telescope.

Since recent years, unmanned aerial systems (UAS) are well-established as sensor platform for small format close range aerial photogrammetry. The unmanned aerial vehicle (drone) is equipped with several navigation sensors, e.g. GNSS and IMU, and remote controlled by a ground-station. Usually, the waypoints of the flight path as well as the trigger points for the camera are scheduled by a flight plan. Due to practical reasons, in this project the camera was controlled remotely by the pilot via video screen.

The equations of the central projection, which transforms three dimensional object coordinates $(X_P\ Y_P\ Z_P)^T$ to corresponding planar image coordinates $(x'\ y')^T$, are given by

$$x' = x'_0 - c\frac{r_{11}(X_P-X_0)+r_{21}(Y_P-Y_0)+r_{31}(Z_P-Z_0)}{r_{13}(X_P-X_0)+r_{23}(Y_P-Y_0)+r_{33}(Z_P-Z_0)} + \Delta x', \tag{1a}$$

$$y' = y'_0 - c\frac{r_{12}(X_P-X_0)+r_{22}(Y_P-Y_0)+r_{32}(Z_P-Z_0)}{r_{13}(X_P-X_0)+r_{23}(Y_P-Y_0)+r_{33}(Z_P-Z_0)} + \Delta y'. \tag{1b}$$

Here, the principal distance c, the principal point x'_0, y'_0 and the distortion effect parameters $\Delta x'$, $\Delta y'$, which compensate for the radial-symmetric lens distortion and the decentring distortion, are known as interior orientation, which are usually constant for all images of a photogrammetric bundle. The parameters of the exterior orientation refer to the image position and orientation w.r.t. the global reference frame and are given by

$$\mathbf{P}_0 = \begin{pmatrix} X_0 \\ Y_0 \\ Z_0 \end{pmatrix}, \qquad \mathbf{R} = \begin{pmatrix} r_{11} & r_{12} & r_{13} \\ r_{21} & r_{22} & r_{23} \\ r_{31} & r_{32} & r_{33} \end{pmatrix},$$

respectively (cf. Luhmann, 2018, Ch. 4.2.1).

The weight of the camera restricts the operating time of the UAS. For that reason, a lightweight 380 g consumer camera Sigma DP3 Merrill was used instead of a heavy high-precision photogrammetric camera. This yields in a flight time of about 25 min. Due to the fact that consumer cameras are not geometrically stabilized, the parameters of the interior orientation were calibrated in-situ during the bundle adjustment for each measurement campaign (e.g. Luhmann, 2018, Ch. 4.4.2).

The image sensor of the camera based on the Foveon chip and captures full color information for each pixel (e.g. Greiwe and Gehrke, 2013). For comparison, the elements of color filter arrays like Bayer pattern are only sensitive for one waveband and the full color is obtained by interpolations (e.g. Verhoeven, 2010). Figure 1 depicts the differences in acquired spectral information between a Foveon based sensor and a color filter array. Full true color information increases the micro-contrast and leads to better image measurements e.g. edge detection during the analysis process. The main reflector surface of ONSA13NE[2], the north-eastern of the Onsala twin telescopes, was equipped by 72 discrete 12-bit coded markers. Additionally, four markers were attached

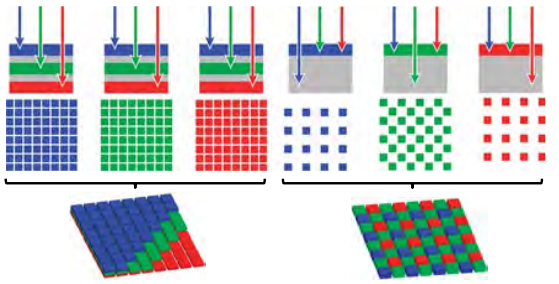

Fig. 1: Differences in spectral information acquirements between Foveon based sensorS (left) and color filter arrays like Bayer pattern (right) (Verhoeven, 2010).

[2] https://youtu.be/sNnHvBaQ3_w

Fig. 2: The VGOS radio telescope ONSA13NE equipped with several coded markers, scale-bars and coordinate cross during the UAS-based photogrammetric survey of the main reflector surface.

at the sub-reflector together with a coordinate cross, which approximately defines the datum of the resulting point clouds by six markers. To transfer the point cloud into a metric system six carbon fiber scale-bars were attached at the sub-reflector, at the strut elements and at the rim of the dish. Figure 2 depicts the prepared main reflector surface of the ONSA13NE during a UAS-based measurement campaign, using a HP-TS960 (HEXAPILOTS).

To obtain a possible deformation pattern of the main reflector, measurement campaigns were carried out redundantly from elevation 0° up to 90° using a step-size of 10° as well as one time in 34°. The flight plan for each elevation angle consists of two flight lines and two concentric spatial circles around the axis of symmetry of the main reflector, cf. Table 1. Figure 3 depicts the established flight plan for elevation angle 30°.

Table 1: Parameter of the flight plan that is used for each measurement campaign. The distances are related to the apex of the main reflector surface.

Type	Traverse (m)	Circle (m)	
Distance	14	14	19
Radius	–	6.5	11.5

Instead of using a configuration where the camera orientation is aligned to the axis of symmetry of the main reflector, the diametrical direction of the main reflector was pointed for each taken image. About 150 suitable images were taken per campaign and analysed by the bundle adjustment software package *AICON 3D Studio*. The software extracts coded markers as well as natural circular targets at the telescope e.g. screws automatically. Thus, more than 500 points are used during the adjustment process per campaign. The uncertainties of the coded markers are between 80 µm and 120 µm w.r.t. the global datum. A detailed description is given by Lösler et al. (2019).

3 Focal length variations

As most of the new VGOS radio telescopes, the main reflectors of the Onsala twin telescopes are designed as rotational symmetric ring-focus paraboloids (e.g. Pantaleev et al., 2017). A ring-focus paraboloid results by combining two quadric surfaces, i.e. a paraboloid and a cylinder. A closed mathematical model of a double-elliptic ring-focus paraboloid was recently derived by Lösler et al. (2017, 2018a,b, 2019) and reads

$$a_1^2(x_i - r_i n_{x,i})^2 + a_2^2(y_i - r_i n_{y,i})^2 = z_i. \qquad (2)$$

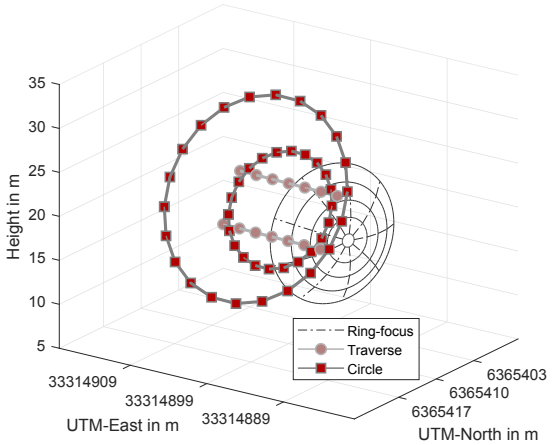

Fig. 3: Established flight plan for elevation angle 30° that consists of two traverses and two circles. The main reflector surface is plotted in the background.

Here, a_1 and a_2 are the parameters of the elliptic paraboloid and $(x_i\ y_i\ z_i)^{\mathrm{T}}$ are the coordinates of the ith point lying on the paraboloid surface. The point-dependent cylinder parameter $r_i = f(b_1, b_2, \phi)$ results from the inverse semi-major and the inverse semi-minor axes b_1 and b_2, respectively, and the cylinder orientation ϕ. The normalized normal vector perpendicular to the cylinder axis is denoted by $\mathbf{n}_i$. In case of a rotational symmetric ring-focus paraboloid, the restrictions $a_1 = a_2$ and $b_1 = b_2$ hold (cf. Lösler et al., 2018a,b). By applying a rotation sequence and a translation, the canonical form is transformed to an arbitrary position in space.

The estimated point sets of each bundle adjustment were corrected for thermal expansions. The parameters of the ring-focus paraboloid were derived by Eq. 2 using a proper errors-in-variables (EIV) solver. For rigorous uncertainties propagation, the dispersion of the estimated point sets was introduced to the EIV to define the a-priori stochastic model of the observations.

Table 2 summarizes the campaign-wise estimated overall RMS values. The panels were adjusted at elevation 34°, thus, smallest deviations can be expected for elevation angles close to 34°. This assumption is confirmed by the estimated RMS values, because larger values can be found close to 0° and 90°, whereas smallest values are given from 30° to 50°.

Table 2: Estimated RMS w.r.t. different survey elevations ϵ.

ϵ	0°	10°	20°	30°	34°	40°	50°	60°	70°	80°	90°
RMS	204	187	200	167	169	192	182	173	178	221	282
in µm	190	194	166	147	–	154	155	162	167	227	292

The paraboloid parameter a yields the focal length via $F = \frac{1}{4a^2}$.

Figure 4 depicts the estimated focal lengths of the 21 measurement campaigns by red dots. Red error-bars indicate the related uncertainties (2σ). The focal length varies in a range of ±1.1 mm and depends on the elevation angle. The maximum occurs at 90°, which confirms the assumption that the main reflector becomes flatter in higher elevation positions (cf. Lösler et al., 2019).

To predict the variations by a suitable function, a common cosine function was adapted, i.e.,

$$F(\epsilon) = 3.7017\,\mathrm{m} - 2.3\,\mathrm{mm}\cos\epsilon. \qquad (3)$$

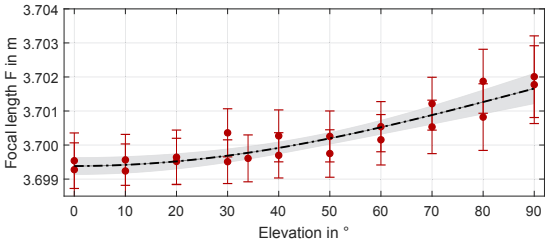

Fig. 4: The estimated focal length of the 21 measurement campaigns with uncertainties (2σ) are illustrated by red dots. The derived prediction function and the related confidence interval (2σ) are plotted in black and grey, respectively.

The resulting prediction function is plotted as black line. The grey colored band indicates the related 2σ confidence.

For comparison, the variations of the focal length are 10-times smaller than reported for conventional radio telescopes (e.g. Sarti et al., 2009; Nothnagel et al., 2013; Bergstrand et al., 2018). The compact-design as well as technological improvements result in a higher rigidity and damped deformations and correspond to the theoretical intention of the VGOS-specifications (Petrachenko et al., 2009).

4 Conclusions

For the fist time, elevation-dependent gravitational deformations of the main reflector of a VGOS-specified radio telescope were studied in detail at the Onsala Space Observatory. The focal length of the north-eastern of the Onsala twin telescopes (ONSA13NE) varies by about ±1 mm and can be predicted by a cosine function.

For this purpose, photogrammetric methods were used to observe the radio telescope in several elevation angles. Instead of using a large crane for data recording, an unmanned aircraft system (UAS) carried out the surveying campaigns. To our knowledge, this was the first time that an UAS is used in radio telescope surveying. The uncertainties of a discrete measured point was about 100 µm and fulfilled the requirements to be at least three times better than the expected variations. Summarized, for free-standing radio telescopes, the UAS provides a promising and practicable surveying method. Neither a crane is required nor additional heavy equipment has to be mounted.

Acknowledgements We thank Lars Wennerbäck and Christer Hermansson for mounting and dismounting the coded markers and the scale-bars at the radio telescope.

This research project is part of the JRP 18SIB01 "Large-scale dimensional measurements for geodesy" (GeoMetre) and has received funding from the EMPIR programme co-financed by the Participating States and from the European Union's Horizon 2020 research and innovation programme.

References

Bergstrand S, M. Herbertsson M, Rieck C, et al. (2018) A gravitational telescope deformation model for geodetic VLBI. *J Geod*, 93(5), 669–680, doi:10.1007/s00190-018-1188-1

Findlay J W (1964) Operating Experience at the National Radio Astronomy Observatory. *Annals of the New York Academy of Sciences*, 116(1), 25–40, doi:10.1111/j.1749-6632.1964.tb33937.x

Greiwe A, Gehrke R (2013) Foveon Chip oder Bayer Pattern - geeignete Sensoren zur Aerophotogrammetrie mit UAS. In: T. Luhmann, C. Schumacher (eds.): *Photogrammetrie - Laserscanning - Optische 3D-Messtechnik: Beiträge der 12. Oldenburger 3D-Tage 2013*, Wichmann, Offenbach, 334–343, ISBN: 978-3879075287

Haas R, Nothnagel A, Schuh H, et al. (1996) Explanatory supplement to the section 'Antenna Deformation' of the IERS Conventions (1996). In: H. Schuh (Eds.): *Explanatory supplement to the IERS conventions (1996)*, Deutsches Geodätisches Forschungsinstitut (DGFI), München, **71**, 26–29

Lösler M, Neidhardt A, Mähler S (2013) Impact of Different Observation Strategies on Reference Point Determination – Evaluations from a Campaign at the Geodetic Observatory Wettzell. In: N. Zubko and M. Poutanen (eds.): *Proc. 21st EVGA Working Meeting*, 255–260, ISBN: 978-951-711-296-3

Lösler M, Eschelbach C, Haas R (2017) Unified Model for Surface Fitting of Radio Telescope Reflectors. In: R. Haas, G. Elgered (eds.): *Proc. 23rd EVGA Working Meeting*, 29–34, ISBN: 978-9188041098

Lösler M, Eschelbach C, Haas R (2018a) Applying Bootstrapping in the Framework of Uncertainty Estimation exemplified by Surface Analysis. *zfv – Zeitschrift für Geodäsie, Geoinformatik und Landmanagement*, 140(4), 224–232, doi:10.12902/zfv-0214-2018

Lösler M, Eschelbach C, Haas R (2018b) Zur Modellierung eines Ring-Focus-Paraboloids. In: T. Luhmann, C. Schumacher (eds.): *Photogrammetrie – Laserscanning – Optische 3D-Messtechnik: Beiträge der 17. Oldenburger 3D-Tage 2018*, Wichmann, Offenbach, 222–234, ISBN: 978-3-87907-643-7

Lösler M, Haas R, Eschelbach C, et al. (2019) Gravitational Deformation of Ring-Focus Antennas for VGOS – First Investigations at the Onsala Twin Telescopes Project. *J Geod*, doi:10.1007/s00190-019-01302-5

Luhmann T (2018) *Nahbereichsphotogrammetrie - Grundlagen, Methoden und Anwendungen*, Wichmann, Berlin, 4th edn, ISBN: 978-3879074792

Mähler S, Klügel T, Lösler M, *et al.* (2018) Permanent Reference Point Monitoring of the TWIN Radio Telescopes at the Geodetic Observatory Wettzell. *avn – Allgemeine Vermessungsnachrichten*, 125(7), 210–219

Nothnagel A, Eichborn M, Holst C (2013) Improvment of focal length results of Effelsberg 100 m radio telescope. In: N. Zubko and M. Poutanen (eds.): *Proc. 21st EVGA Working Meeting*, 55–59, ISBN: 978-951-711-296-3

Pantaleev M, Haas R, Billade B, et al. (2017) Onsala Space Observatory – IVS Technology Development Center Activities during 2015-2016. In: K. D. Baver, D. Behrend, and K.L . Armstrong (eds.): *International VLBI Service for Geodesy and Astrometry 2015+2016 Biennial Report*, 301–305, NASA/TP-2017-219021

Petrachenko B, Niell A, Behrend D, et al. (2009) Design aspects of the VLBI2010 system. NASA/TM-2009-214180

Sarti P, Vittuari L, Abbondanza C (2009) Laser Scanner and Terrestrial Surveying Applied to Gravitational Deformation Monitoring of Large VLBI Telescopes' Primary Reflector. *J Geod*, 135(4), 136–148, doi:10.1061/(ASCE)SU.1943-5428.0000008

Süß M, Koch D, Paluszek H (2012) The Sardinia Radio Telescope (SRT) optical alignment. *Proceedings of Ground-based and Airborne Telescopes IV*, 8444, 84442G-1–84442G-16

Verhoeven G J J (2010) It's All about the Format – Unleashing the Power of RAW Aerial Photography. *Int. J. Remote Sens.*, 31(8), 2009–2042, doi:10.1080/01431160902929271